Multifractal Spectrum Observed in the Distribution of Galaxies of the Updated Redshift Catalog

W. M. Macek[1,2],

and

D. Wójcik [2,1]

Received _____; accepted _____

July 31, 2024 to be submitted to ApJS

[1]Institute of Physical Sciences, Faculty of Mathematics and Natural Sciences, Cardinal Stefan Wyszyński University, Wóycickiego 1/3, 01-938 Warsaw, Poland, https://orcid.org/0000-0002-8190-4620

macek@uksw.edu.pl

[2]Laboratory for Solar System Physics and Astrophysics, Space Research Centre, Polish Academy of Sciences, Bartycka 18 A, 00-716 Warszawa, Poland

macek@cbk.waw.pl

ABSTRACT

We have recently argued that a simple nonlinear law could possibly be important for the origin of the Universe resulting in fractal or multifractal features. Various fractal scaling models of the large-scale mass distribution have already been proposed. The expected universal multifractal function for galaxies is similar to that identified by NASA's Voyager mission in the Solar System. Hence we now apply the similar method for determination of the reliable multifractal spectrum of distribution of galaxies on cosmological scales, based on selected observations from a million of galaxies in the Redshift Catalog updated in June 2008. We show that the observed spectrum is consistent with the weighted one- or two-scale Cantor set models characteristic for turbulence in laboratory and inside the Sun's heliosphere immersed in the very local interstellar medium. However, the total degree of multifractality $\Delta \approx 0.2$ is smaller than that inside the heliosphere. This would be characteristic for a simple linear fractal scaling of galaxy distribution, but somewhat varying for nearby ($\Delta \simeq 0.1$) and the most remote galaxies ($\Delta \simeq 0.2$) receding from our Solar System. The parameters $p \approx 0.45$ and $\lambda \leq \frac{1}{2}$ for one-scale model are apparently related to some voids in the large-scale distribution of matter. A possible asymmetry ($A \sim 3/4$) of the total spectrum for the two-scale weighted Cantor set ($A \neq 1$) could admittedly be attributed to some deviations from the Hubble's law for the ideal uniform expansion of the Universe.

Subject headings: scaling: multifractals – universe – galaxies: clustering – mass distribution

1. Introduction

In the eighteen century Immanuel Kant suggested that some nebulae might be distant systems of stars, but the first galaxy beyond the Milky Way Galaxy was discovered only in 1924. In fact, by the early twentieth century, based on observations using 2.5-meter and 5-meter telescopes on Mount Wilson and Palmer Mountain, respectively, Edwin Hubble has established the view the expanding Universe with galaxies receding from the Solar System, with velocities roughly proportional to their celestial distances. At present, after the past one hundred years, one can estimate that even a trillion of galaxies, $(0.2 - 2) \times 10^{12}$, may exist in the entire Universe. Because of, e.g., the problem of dark matter raised nearly half a century ago, not all the galaxies can admittedly be observed directly, but some fractions of them are now classified and well catalogued. Anyway, this allows us to study in more detail the large-scale structure of the distribution of galaxies in the Universe.

It is well known that the Euclidean three-dimensional space filled-up with a constant density of mass distribution would have produced the infinite Newtonian gravitational forces. Admittedly, despite the discovery of large massive inhomogeneous structures with large spatial empty voids, which are common features of astrophysical observations, the standard cosmological model based on the theory of general relativity also employs a somewhat similar approximation claiming that the Universe is homogeneous, at least on some very large scales. On the other hand, the available data satisfy power law distributions of mass with various exponents that are substantially lower than three, ranging from a value greater than 1 to about 2 (Mandelbrot 1982, chapter III). This would correspond to special values of various fractal dimensions (Macek 2020, ch. 3.3), (Macek 2022, ch. 4). The fractal view of galaxy clusters is supported by luminous radiation data and is consistent with a flat Universe in thermodynamic equilibrium; in addition, this certainly satisfies the Copernican principle.

Some simple monofractal distributions of galaxies have been reported in the astrophysical literature (e.g., Maddox 1987; Teles et al. 2022), but it seems that the clustering structures with number $N(l)$ at distance l are better explained by the multifractal spectrum of dimensions $f(\alpha)$ with $N(l) \propto l^{-f(\alpha)}$ (e.g., Jones et al. 1988; Gaite 2021). The richness of various fractal scaling behavior has been exploited by Jones et al. (2005). Interestingly, the universal multifractal function for galaxies is similar to that identified by NASA's Voyager missions at the heliospheric boundaries (see Macek et al. 2014) (as more recently analyzed even on very small kinetic scales in the Solar System's plasmas (e.g., Macek et al. 2018, 2023; Wójcik & Macek 2024)). Therefore, we apply the similar fractal numerical methods here for direct determination of the multifractal spectrum of distribution of galaxies on cosmological scales, using the best currently available catalog. We show that the observed multifractal spectrum is basically consistent with a one-scale Cantor model characteristic for turbulence in space and laboratory.

2. Catalog of Galactic Data

We have used in our analysis the data of redshifts obtained from the Smithsonian Astronomical Observatory Telescope Data Center available from `http://tdc-www.harvard.edu/zcat/velocity.dat`. Instead of the older *CfA* catalog with only 359 objects and the apparent magnitudes $m \leq 14.5$, as analyzed by Martinez et al. (1990), we have now looked at the Updated (June 2008) CfA Redshift Catalog *UZCAT* (*ZCAT*) compilation of a million (from a trillion) of various observed galaxies, see `http://tdc-www.harvard.edu/zcat/zcom.htm`. This catalog originally consisted of various sets of galaxies (e.g., NZ40, SDSS, 2dF, 6dF, and ZCAT), and later other published observed data on some galaxies has been added by the catalogue authors (e.g., Shectman et al. 1996; Skrutskie et al. 2006; Jones et al. 2009). But we have not used velocities with

negative source designations (19, 517 observations), which are in private domain (and hence cannot be used without the owner's consent).

After all, the data assembled by various authors for studying the large-scale structure of the Universe are basically complete in redshift information, but not necessarily in some other terms like diameter, magnitude and references. However, the velocities listed are the best available with respect to the quoted measurement errors and the reliability of the source. Surely, the purpose of this catalog is to be a complete list of galaxies with radial velocities for mapping and statistical studies. Incidentally, following remark that users should remove objects of type > 20, which were misclassified as galaxies, before using this galaxy catalog, 14, 177 observations of V_H have been omitted. The most frequent type was 25 – a plate flaw, stars, and other misclassifications.

We have used here the radial velocities $V_H(r) < c$, with light speed $c = 299\ 792\ 458$ m s^{-1}, for a relativistic redshift $z = \sqrt{\frac{1+V_H/c}{1-V_H/c}} - 1$ (see, e.g. Antonyuk 2020), which in a nonrelativistic limit of $V_H \ll c$ is $z \approx V_H/c$, can somewhat be corrected for the motion of the Sun, with the apex velocity of ∼230 km s^{-1}, right ascension (RA) 18 h 28 m and declination (Dec.) +30 deg (North in galactic coordinates). Therefore, we have (cf. Davis & Lineweaver 2004)

$$V_H = \begin{cases} c\,z & \text{for } V_H \ll c, \\ c\,\frac{(1+z)^2-1}{(1+z)^2+1} & \text{otherwise.} \end{cases} \tag{1}$$

and the heliocentric distance to any galaxy is given by $L_H := \frac{c}{H_0} \ln(1+z) = \frac{c}{2H_0} \ln \frac{1+V_H/c}{1-V_H/c}$, and for $z \ll 1$ is $L_H \approx \frac{cz}{H_0}$, or $L_H \approx V_H/H_0$, assuming a Hubble parameter (present epoch) $H_0 = 70$ km s^{-1} Mpc $^{-1}$.

Strictly speaking, we have gotten rid of negative (blushifted) redshifts z, eliminated data gaps ($\sim 50,000$ blank velocities), and removed outliers using the IQR method, which is useful for skewed data (in contrast to usual Z-score method), i.e., IQR $= Q_3 - Q_1$, where

$Q_{1,3}$ are the first and third quartiles correspondingly, and then the outliers are defined as observations falling below $Q_1 - 1.5\,\mathrm{IQR}$, or above $Q_1 + 1.5\,\mathrm{IQR}$. Thus, we have analyzed the sample of $783,152$ observations down to magnitude $m \lesssim 29.5$ (as limited by the Hubble Space Telescope) and very high relativistic velocities. After all, one can confirm that for the currently estimated diameter of the Universe of about $2R_{\mathrm{max}} \approx 28.5$ Gpc, the maximum receding velocity in most remote galaxies in the last category denoted by violet should be $V_{max} = c\tanh(2R_{max}H_0/c) = 293,018$ km s^{-1} (with $V_H/c = 0.98$ and a very large redshift $z_{max} \approx 8.35$).

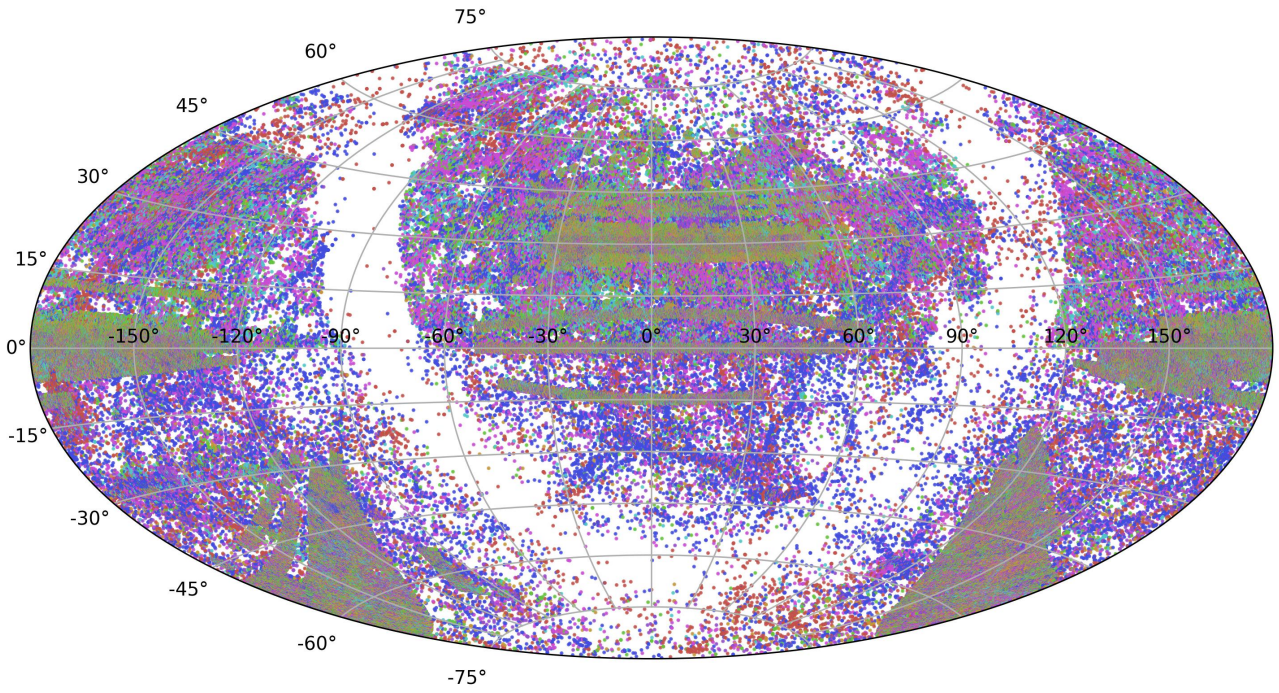

Fig. 1.— The sky map of different categories of galaxies: red, blue, magenta, cyan, green, orange, and violet depending of the redshifted velocity as used in the UZCAT updated (2008) catalogues.

The plot map on the sky of all the analyzed galaxies of *UZCAT* (Aitoff projection) is illustrated in Figure 1, for the following various categories of nearby and more and

more distant remote galaxies: red, blue, magenta, cyan, green, orange, and violet. To construct the map, we have used here right ascension and declination in the Galactic (J2000) coordinate system (centered at 0° increasing to the left). In particular, the green and orange groups represent the well studied regions of the 2dF GRS (initially 100,000, up to 380,000 datapoints) `http://www.2dfgrs.net`. The other SDSS DR3 Survey `https://classic.sdss.org/dr3/` consists of $\sim 350,000$ galaxies and then we also have the LCRS and the Century surveys, as extensively studied by John Huchra and Zwicky. The clusters rely on published finding charts, and these clusters are standardized by ID's using Dressler's (1980) numbers.

Apparently, the observable universe, with possible hundreds billion large galaxies, is not a chaotic scatter. The galaxies form intricate filaments and other large structures, shaping a web-like pattern that defines the large-scale structure of the cosmos. This pattern reflects the behavior of dark matter and provides insights into the Universe's overall structure and evolution. Obviously, differences in population of each category of galaxies could result in specific somewhat different fractal and multifractal characteristics, Table 1.

In Figure 2 box plot of various populations for the following categories of the galaxies under study: red, blue, magenta, cyan, green, orange, and violet are displayed depending of the receding speed together with the empirical probability density functions (PDFs), which have been computed by using kernel density estimates (KDE). All the KDE plots show generally low densities across different ranges. They exhibit minor but no dominant peaks, indicating a multimodal distribution with several small clusters. The data points appear to be spread out evenly across the ranges, with no significant concentration. The skewness is well pronounced in the contrasting cases.

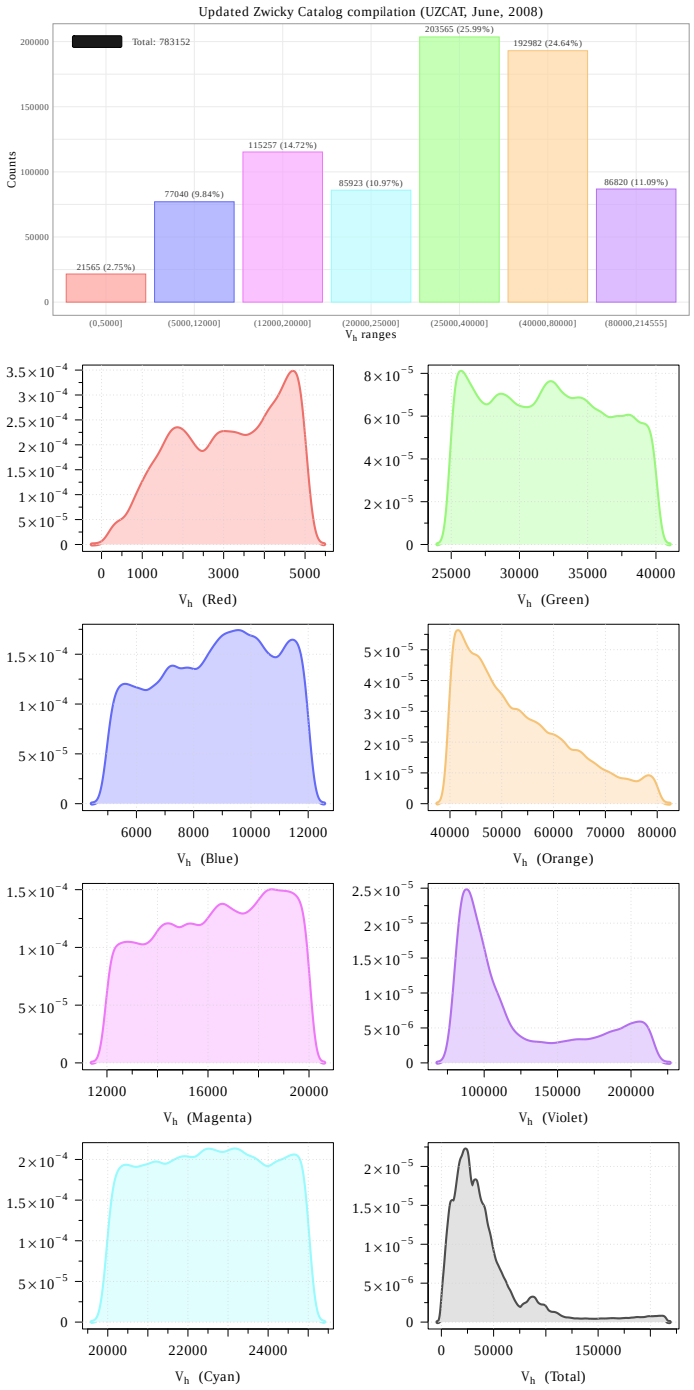

Fig. 2.— The box plot of distribution and probability density functions (PDFs) of different colored categories of galaxies red, blue, magenta, cyan, green, orange, and violet depending of the receding speed of the UZCAT updated (2008) catalog with populations displayed in Table 1.

3. Multifractal Analysis

The basic concepts of fractal sets are elucidated in textbooks (e.g., Falconer 1990; Ott 1993; Macek 2020). We only note here that fractals are characterized by *self-similarity*, which is described by a single fractal dimension (independent of scale l). On the other hand, a multifractal is a more complex object that exhibits different self-similarities (dependent on scale), which is described by the spectrum of dimensions or a multifractal singularity spectrum.

3.1. Multifractal Characteristics

A comparison of the main characteristics of fractals (with a usual measure of the volume of a set) and multifractals (with a probability measure to visit a fraction of the set) has been thoroughly discussed by Macek et al. (2014) in Sec. 2.1.

As is known, contrary to a usual monofractal scaling, basically two universal functions are characteristic for multifractals. Namely, for a set consisting of N elements with probability measures $p_i(l)$ associated with a given scale l, the generalized dimension is

$$D_q = \frac{1}{q-1}\lim_{l\to 0}\frac{\ln\sum_{i=1}^{N}(p_i)^q}{\ln l} \tag{2}$$

while the multifractal singularity spectrum $f(\alpha)$ as function of a singularity strength α ($p_i(l) \propto l^{\alpha_i}$) is defined by

$$f(\alpha) = \lim_{\varepsilon\to 0}\ \lim_{l\to 0}\frac{\ln[N_l(\alpha+\varepsilon) - N_l(\alpha-\varepsilon)]}{\ln 1/l} \tag{3}$$

In general, the generalized dimensions D_q are nonlinear functions of any given real index q, and provide important information about multifractality of the system (Ott 1993). Equivalently, the universal singularity spectrum $f(\alpha)$, with the maximum value $f(\alpha_0) = D_0$, characterize multifractality of the system under study (Falconer 1990). The line joining

the origin to the point $f(D_1) = D_1 = \lim_{l\to 0} \sum_{i=1}^{N} [p_i(l) \log(p_i(l)]/\log(l)$ is tangent to the shape of the spectrum. These functions illustrated in Figure 3.7 of Macek (2020), as thoroughly discussed by Macek et al. (2011) and Macek et al. (2012), allow a comparison of the experimental results with the phenomenological models of turbulence (Frisch 1995; Biskamp 2003).

In addition to a usual probability measure $p_i(l)$, we can also use the following higher-order pseudoprobability measures associated with each scale l:

$$\mu_i(q,l) \equiv \frac{p_i^q(l)}{\sum_{i=1}^{N} p_i^q(l)}. \tag{4}$$

In this way, (using a fractal dimension index $f_i(q,l) \equiv \log \mu_i(q,l)/\log l$), one can directly calculate the multifractal spectrum as the average of the pseudoprobability measure $\mu_i(q,l)$ according to Equation (4) indicated by the squared brackets $\langle \cdots \rangle$ (Chhabra & Jensen 1989)

$$f(q) \;\equiv\; \lim_{l\to 0} \sum_{i=1}^{N} \mu_i(q,l)\; f_i(q,l) = \lim_{l\to 0} \;\frac{\langle \log \mu_i(q,l) \rangle}{\log(l)}. \tag{5}$$

The average value of the singularity strength is given by Chhabra et al. (1989)

$$\alpha(q) \;\equiv\; \lim_{l\to 0} \sum_{i=1}^{N} \mu_i(q,l)\; \alpha_i(l) = \lim_{l\to 0} \;\frac{\langle \log p_i(l) \rangle}{\log(l)}. \tag{6}$$

4. Multifractal Model

Macek & Strumik (2014) and Macek (2022) have argued that simple nonlinear or fractal models provides a useful tool for phenomenological analysis of complex turbulent media. For example, the generalized weighted Cantor set is a simple example of multifractals, as explained, e.g., by Falconer (1990). This model is illustrated in Figure 2 of Macek (2007). When constructing this model with scale parameter $\lambda \leq 1/2$ we have the analytical expressions for D_q and $f(\alpha)$ (e.g. Macek & Wawrzaszek 2009). Namely, if measures p

and $1-p$ are applied to the left and right remaining parts of a unit interval the function $\tau(q) \equiv (q-1)D_q$ is equal to (Macek et al. 2012, Equation 11)

$$\tau(q) = \frac{\ln[p^q + (1-p)^q]}{\ln \lambda} \tag{7}$$

and for $\alpha(q) = \tau'(q)$ we have the following formula:

$$\alpha(q) = \frac{1}{\ln \lambda} \, \frac{p^q \ln p + (1-p)^q \ln(1-p)}{p^q + (1-p)^q}. \tag{8}$$

Then, using the Legendre transformation, we obtain the explicit formula for the multifractal spectrum $f(\alpha(q)) = q\alpha(q) - \tau(q)$.

However, for a more developed generalized two-scale weighted Cantor set we must specify two scales l_1 and l_2 ($l_1 \neq l_2$), satisfying $l_1 + l_2 \leq 1$. In this case, one needs to solve for $\tau(q)$ the transcendental equation (e.g., Ott 1993),

$$\frac{p_1^q}{l_1^{\tau(q)}} + \frac{p_2^q}{l_2^{\tau(q)}} = 1, \tag{9}$$

which is only somewhat more general than the analytical solution given by Equation (7). Finally, it is worth to mention that the standard middle-thirds monofractal Cantor set model is recovered only for $\lambda = 1/3$ and $p = 1/2$, with $D_0 = \ln 2 / \ln 3$.

The difference between the calculated maximum and minimum dimensions, related to the respective regions in the phase space with the least and most dense probability densities has been proposed by Macek (2007) and Macek & Wawrzaszek (2009)

$$\Delta \equiv \alpha_{\max} - \alpha_{\min} = D_{-\infty} - D_{\infty} = \left| \frac{\log(1-p)}{\log l_2} - \frac{\log(p)}{\log l_1} \right| \tag{10}$$

as a degree of multifractality. Naturally, this parameter Δ exhibits a deviation from a strict self-similarity, and it can also be used as a degree of intermittency as explained in (Frisch 1995, ch. 8). The next quantitative parameter, describing the multifractal scaling, is the measure of asymmetry of the spectrum defined by Macek & Wawrzaszek (2009)

$$A \equiv \frac{\alpha_0 - \alpha_{\min}}{\alpha_{\max} - \alpha_0}, \tag{11}$$

where $\alpha = \alpha_0$ is the point at which the spectrum has its maximum, $f(\alpha_0) = D_0$. The case when $A = 1$ ($l_1 = l_2 = 1/2$) corresponds to the one-scale p-model (e.g., Meneveau & Sreenivasan 1987).

Now, following Burlaga (1995) the probability measures $p(l)$ depending on scale $l := L_H$, as discussed in Sec. 2, can be constructed using observed distribution of galaxies. Namely, first normalizing a series of the average number of the observed objects $n(l_i)$ in i-th shell of radius l_i, where $i = 1, \ldots, N = 2^m$ (e.g., taking $m = 17$) for $j = 2^{m-k}$, $k = 0, 1, \ldots, m$

$$p(x_j, l) \equiv \frac{1}{N} \sum_{i=1+(j-1)\Delta l}^{j\Delta l} n(l_i) = p_j(l), \tag{12}$$

is calculated with the successive average values $\langle n(l_i + \Delta l)\rangle$ of $n(l_i)$ between l_i and $l_i + \Delta l$, for each $\Delta l = 2^k$ with the total N number of galaxies in the system (cf. Macek et al. 2011).

One can show that in the inertial range of scales the average value of the qth moment of p at various scales l should scale as (Burlaga 1995)

$$\langle p^q(l)\rangle \sim l^{\gamma(q)}, \tag{13}$$

where the exponent γ is related to the generalized dimension, $\gamma(q) = (q-1)(D_q - 1)$. Following this method, using these slopes for each real q, the values of D_q can be determined, Equation (13). Alternatively, as explained in Section 3, the multifractal function $f(\alpha)$ versus scaling index α, which exhibits universality of the multifractal scaling behavior, can be obtained using the Legendre transformation. It is worth noting, however, that we obtain this multifractal universal function directly from the slopes given in Equations (5) and (6), using this direct method in various situations (see, Macek & Wawrzaszek 2009; Macek et al. 2011, 2012, 2014).

5. Results

Admittedly, with the *CfA* limited observations, one can only determine the points near the maximum of $f(\alpha)$ (cf. Martinez et al. 1990). One can possibly extrapolate these points near the intercepts at the maximum, $f(\alpha_0) = D_0$. On the other hand, in our study based on much more copious *UZCAT* data one can find more reliable multifractal spectrum of the distribution of galaxies in the Universe.

Therefore, we consider astronomical surveys at different right ascension (RA) and declination (Dec) values, as seen in Figures 1 and 2. But, first instead of plotting observations by the exact positions on the celestial sphere (which would not be exactly insightful), we show how a given property changes on a plot by RA. We have used this variable as a proxy for time in a series of heliocentric velocities for individual galaxies involves treating the $0 - 24$ h range of RA (similarly to a 24-hour time period), but now in the J2000 galactic frame of reference. This plot created using a right ascension (celestial equivalent of longitude) variable is commonly constructed in context of observational astronomy, when tracking the position of celestial objects over time. Obviously, this leverages the regular rotation of the Earth to map RA values to observational time, assuming observations are evenly distributed.

In this way, Figure 3 displays differences of successive 2^n-step averages of large-scale fluctuations in the receding redshifted speeds $\Delta_{2^n} V_H$ (in km s^{-1}) for $n = 5, \ldots, 12$, compare (Burlaga 1995, Fig. 9.7). One can identify patterns or trends, which may correspond to certain celestial regions or astronomical phenomena. Moreover, any deviations from the ideal linear Hubble's law can provide insights into large-scale structures, peculiar motions, and evolutionary effects. In particular, we see some irregular bursty, spiky, inhomogeneous (aperiodic, and asymmetric) features (of varying widths) that are characteristic for multifractal fluctuations for intermittent turbulence. In most cases the magnitudes of

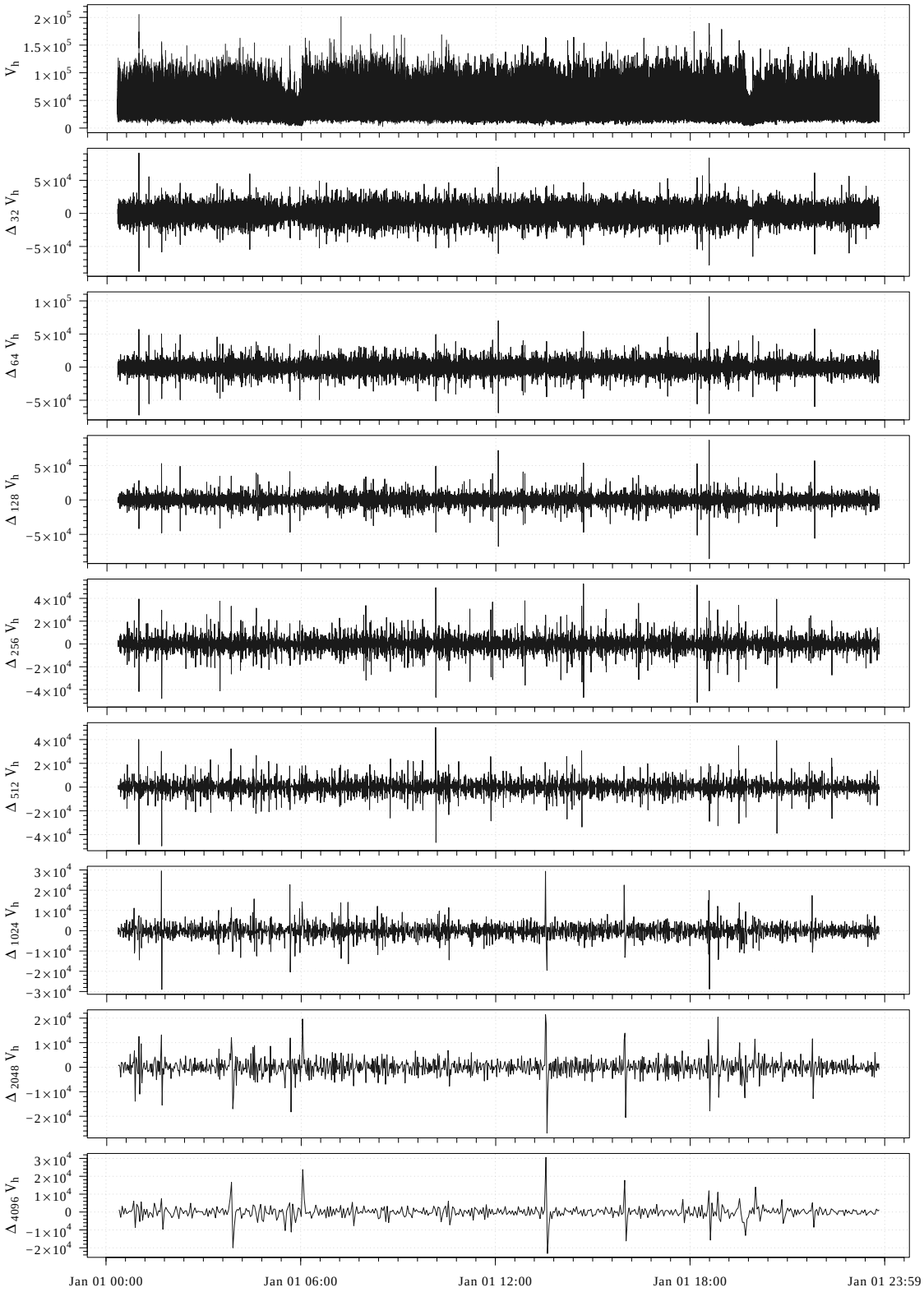

Fig. 3.— The differences of successive 2^n-step averages $\Delta_{2^n} V_H$ [km s^{-1}] of large-scale speed fluctuations for $n = 5, \ldots, 12$ using observed distribution of galaxies based on the selected *UZCAT* data.

positive fluctuations are somewhat greater than those for the negative fluctuations. Because time series for larger scales are magnified parts of the time series for the velocity increments on smaller scales, it seems that the cosmological fluctuations are self-affine on different scales. Hence we can proceed with the multifractal analysis for various q values and scales l. The probability measures $p(l)$ depending on scale $l := L_H$ of Sec. 2 (normalized) is now constructed according to Equation (12) for each category as obtained using the *UZCAT* galaxy catalog data in Figure 1.

Second, in Figures 4 and 5 both average logarithmic probability and pseudoprobability measures $\langle \log_{10} p_i(l) \rangle$ and $\langle \log_{10} \mu_i(q,l) \rangle$ versus $\log_{10} l$ for the all colored categories in the *UZCAT* catalog are now presented for the following (positive and negative) values of q: 6, 5, 4, 3, 2, 1, 0, -1, -2, -3, -4. (Values of q featuring fittings with $R^2 < 0.975$ and $r < 0.975$ have been rejected, where r denotes the Pearson correlation coefficient). As we see, the calculated slopes can be fitted to straight lines in the range of scales typically of to 4 even up 5 orders of magnitude. Hence, similarly as for the heliospheric plasma cf. (Macek & Wawrzaszek 2009; Macek et al. 2012, 2014), we can obtain the multifractal spectrum using *UZCAT* data and compared the observational points with the weighed one-scale or the two-scale Cantor set models as discussed in Section 4.

The generalized dimensions D_q as a function of q and the universal singularity spectrum $f(\alpha)$ as functions of singularity strength α are finally displayed in Figure 6 and 7, respectively. The values of D_q and $f(\alpha)$, as given in Equations (5) and (6), are calculated using the *UZCAT* data (denoted by boxes) and compared with both Cantor set models (cf. Macek 2007, Figure 3). In particular, we have $f(\alpha_0) := D_0 = 1.0$ and $D_1 \lesssim 1.0$. We see that the catalogued observations are reasonably well consistent with the p-model or one-scale Cantor set symmetric spectrum (continuous lines), fitted to the theoretical solutions of Equations (7), especially for $q > 0$ (left part of the spectrum) and still somewhat less clearly

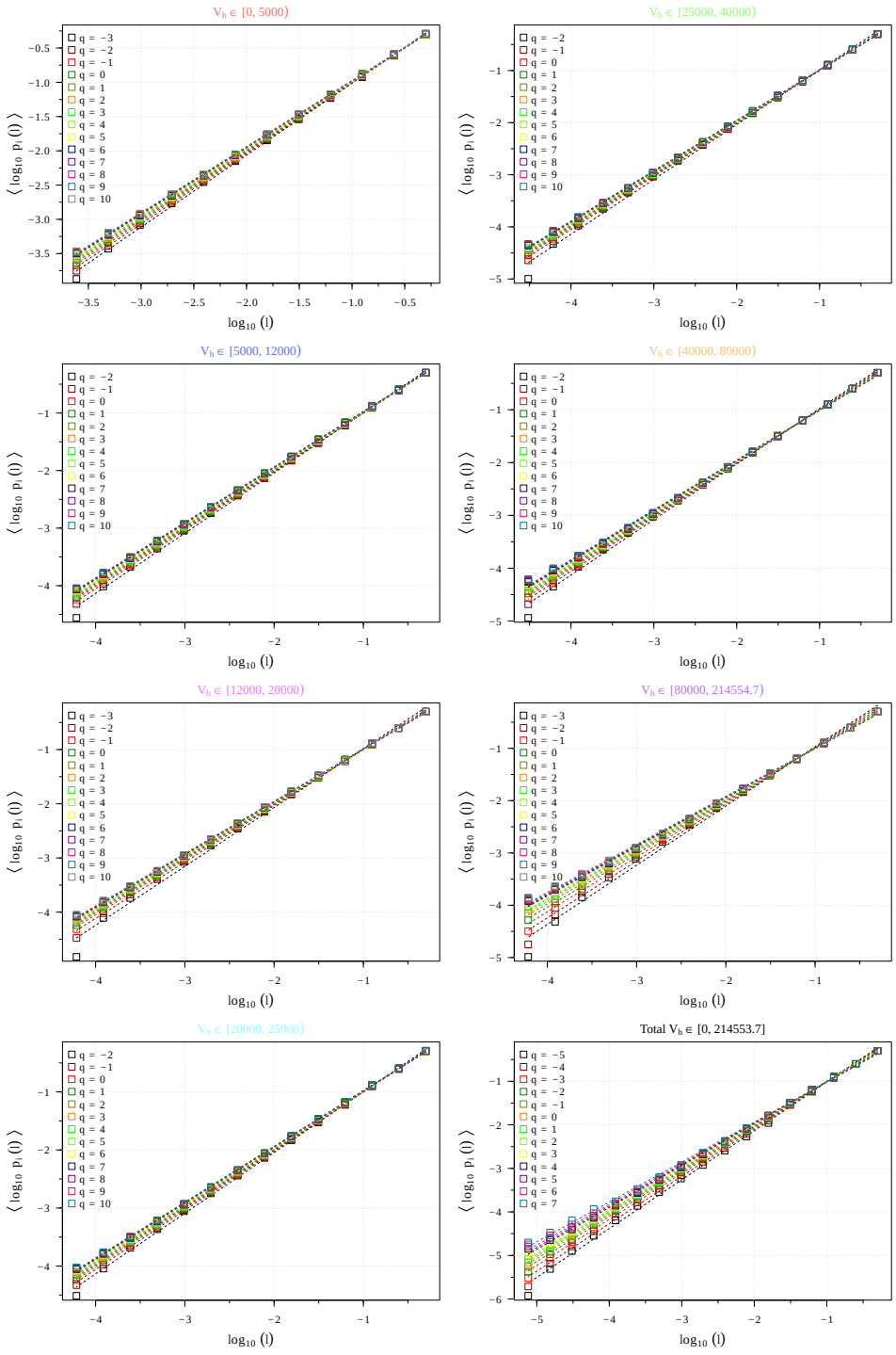

Fig. 4.— Generalized average logarithmic probability $\langle \log_{10} p_i(l) \rangle$ (a) depending on $\log_{10} l$ for $-4 \leq q \leq 6$. These results are obtained using the *UZCAT* catalog.

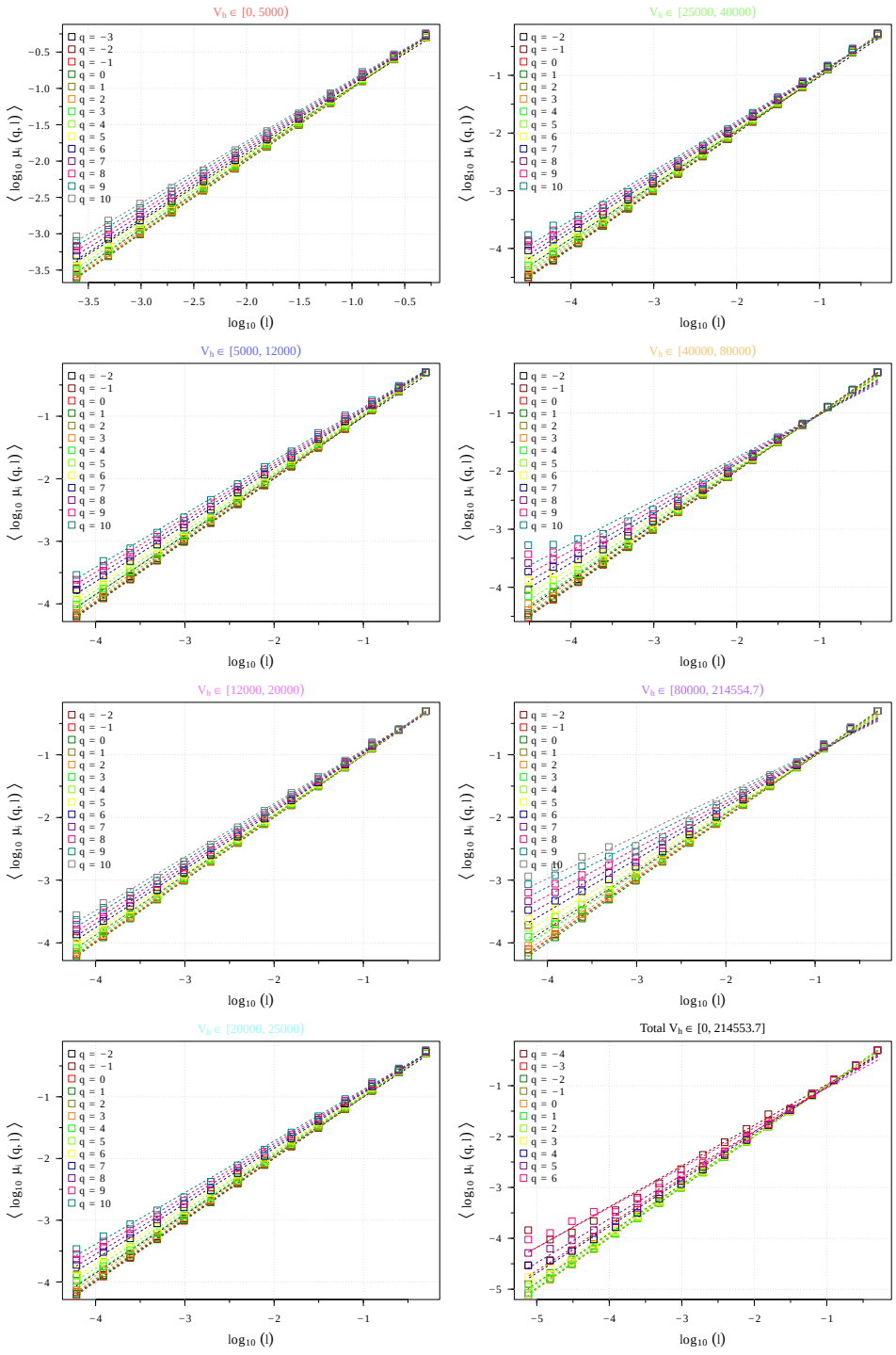

Fig. 5.— Generalized average logarithmic pseudoprobability $\langle \log_{10} \mu_i(q,l) \rangle$ depending on $\log_{10} l$ for $-4 \leq q \leq 6$. These results are obtained using the *UZCAT* catalog.

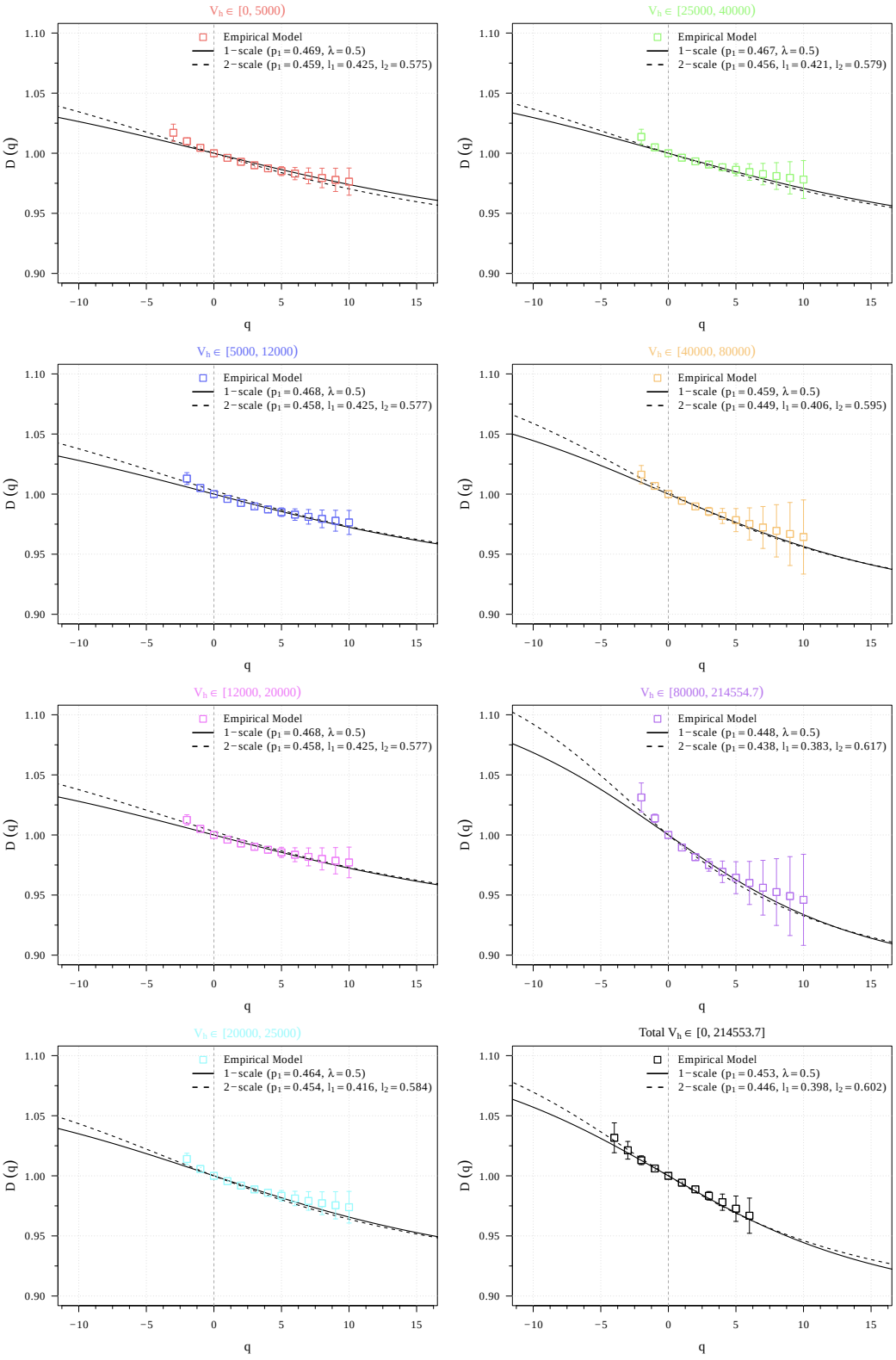

Fig. 6.— The obtained generalized dimensions D_q as functions of q and for the observation categories of data in the *UZCAT* catalog compared with the one-scale (continuous lines) or the two-scale (dashed lines) weighted Cantor models.

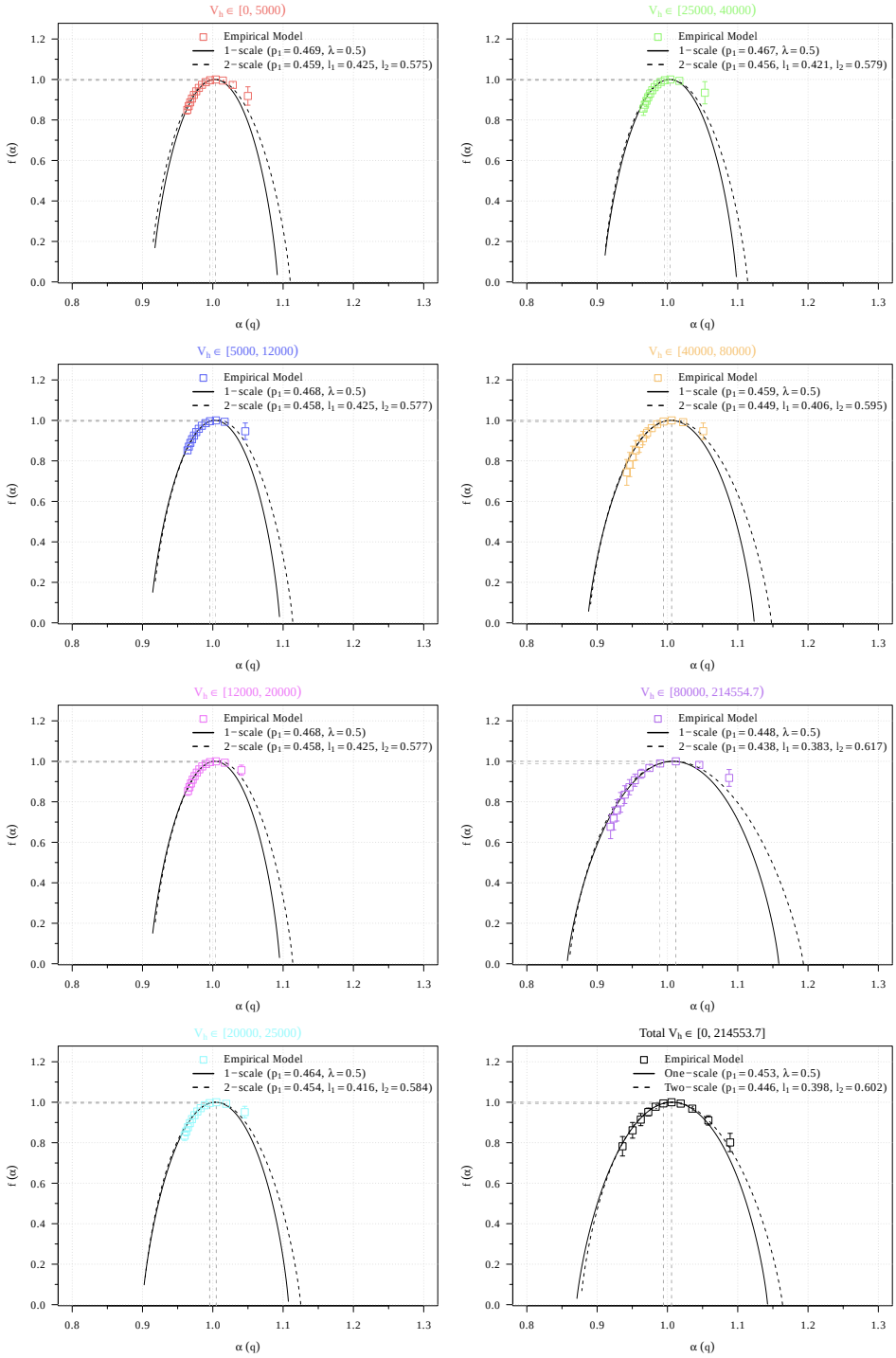

Fig. 7.— The obtained multifractal measures od the multifractal spectrum $f(\alpha)$ as function of the singularity strength α (boxes) for the various observation data of the *UZCAT* catalog compared with the one-scale (continuous lines) or the two-scale (dashed lines) weighted Cantor models.

for $q < 0$ (right side).

Naturally, a somewhat even better agreement is seen with the asymmetric two-scale (dashed lines) Cantor set model, with the corresponding parameter p (or $p_1 = p$, and $p_2 = 1 - p_1$) including l_1 and l_2 of the theoretical model given by Equation (9). Hence the empirical values are in a good agreement with the theoretical model (Macek 2020, Fig. 3.7). To select correctly, all these model parameters (p_1, p_2, l_1, l_2), we have used the Huber's loss metrix (1964) to find the best possible fits. The method combines the MSE and MAE metrics, giving a better loss function that is less sensitive to outliers, e.g., due to irregular intervals in the time series. Further, for the two-scale Cantor model (as well as for the one-scale model), we have $p_1 + p_2 = 1$ (see also Figure 3.9 of Ref. (Macek 2020)), so the fragmentation with probability p_1 among the fragment of length l_1 is virtually the same as with p_2 under l_2.

However, the total degree of multifractality $\Delta \approx 0.2$ is substantially smaller then that inside the heliosphere $\Delta = 0.3 - 0.7$, but larger than that in nonmultifractal ($\Delta \approx 0$) case of the very local interstellar medium (VLISM) after the crossing of the heliopause (at ~ 122 AU) by Voyager 1 in 2012 (Macek et al. 2014). This would rather indicate toward a simple linear fractal scaling of distribution for all the galaxies. Anyway, the parameters $p \approx 0.45$ and $\lambda \leq \frac{1}{2}$ for one-scale model are apparently related to some voids in the large-scale distribution of matter. In particular, the calculated slightly asymmetric spectra with $A = 0.5 - 1.4$ for two-scale weighted Cantor set model ($A \neq 1$) could be related to the deviation from Hubble's law for the uniformly expanding Universe.

Therefore, we have also calculated the multifractal parameter Δ and asymmetry A of Equations (10) and (11) in the observed Universe depending on the distances for all the categories: red, blue, magenta, cyan, green, orange, and violet, which are provided in Table 1. The obtained differences listed in Table 1 are somewhat varying (from 0.1

Table 1: Values of Parameters Describing Multifractality Δ and Asymmetry A of the Spectra for the Redshifts from the *UZCAT* Catalog for Variously Populated Categories of Distances to Remote Galaxies (in 10^3 km s^{-1}).

Galactic Category	**Velocity max**	**Population**	**Multifractality** Δ	**Asymmetry** A
Red	5	21,556	0.0862	0.8817
Blue	12	77,026	0.0822	0.9677
Magenta	20	115,233	0.1225	0.4774
Cyan	25	85,905	0.0855	1.1093
Green	40	203,561	0.0873	0.7793
Orange	80	192,982	0.1087	1.4238
Violet	< 300	86,820	0.2133	0.7711
Total		783,152	0.2045	0.7493

to 0.2) for nearby ($\Delta \simeq 0.1$) and the most remote galaxies ($\Delta \simeq 0.2$) receding from our Solar System. This should be attributed to variation in the population of receding galaxies in various categories according to their distances. The parameters $p \approx 0.45$ and $\lambda \leq \frac{1}{2}$ for one-scale model are apparently related to some voids in the large-scale distribution of matter. A possible asymmetry ($A = 0.75$) of the total spectrum for the two-scale weighted Cantor set ($A \neq 1$) could admittedly be attributed to some deviations from the Hubble's law for the ideal uniform expansion of the Universe.

6. Conclusions

In summary, in this Letter, based on a sample consisting of various categories of about $800,000$ galaxies taken from the *UZCAT* catalog, as highlighted by colors in Figure 1, for the large-scale distributions of all galaxies existing in the Universe, we have studied intermittent self-affine multifractal fluctuations in the averages heliocentric (relativistic redshifted) velocities, as presented in Figure 3.

Basically, using the calculated slopes depicted in Figure 4 and the one-scale or two-scale weighted Cantor set models, we have finally obtained the generalized dimensions and the universal multifractal spectrum shown in Figures 6 and 7. The model parameters $p \lesssim \frac{1}{2}$ and $\lambda \leq \frac{1}{2}$ of Equation (7) are apparently related to some voids in the large-scale distribution of matter in the Universe. In this way, we have provided a new supporting important evidence that the large-scale galaxy distribution most probably has multifractal structure consistent with the weighted one-scale Cantor set model.

Because of the differences in population of various classes of galaxies, the degree of multifractality Δ of the spectrum somewhat varies between 0.1 and 0.2 for the more and more remote receding distances, as listed Table 1, a possible asymmetry $A \sim \frac{3}{4}$ of the total

spectrum may be caused by the deviations from the ideal Hubble's law. However, the degree of multifractality is rather small, $\Delta \lesssim 0.2$, as obtained for admittedly a tiny fraction of all possibly existing galaxies. Hence one is still not able to give any definitive answer weather the galaxies in the entire Universe should actually exhibit multifractal or even a simple fractal distribution, as has already been suggested by Mandelbrot (1982).

We thank Maciej Bzowski from the Space Research Center for discussion on the astronomical catalog data, Vincenzo Carbone from the University of Calabria and Len F. Burlga from the NASA Goddard Space flight Center for help in methods of fractal analysis. The influential contribution of John Huchra (1948–2010) to the galaxy catalog should be acknowledged. The sky map of the selected galaxies has been constructed by using the *AstroPy* package for Astronomy in Python. Data have been processed using statistical programming language R.

This work has been supported by the National Science Centre, Poland (NCN), through grant No. 2021/41/B/ST10/00823.

ORCID iDs

W. M. Macek `https://orcid.org/0000-0002-8190-4620`

`http://www.cbk.waw.pl/~macek`

D. Wójcik `https://orcid.org/0000-0002-2658-6068`

REFERENCES

Antonyuk, P. 2020, Journal of Physics: Conference Series, 1557, 012039

Biskamp, D. 2003, Magnetohydrodynamic Turbulence (Cambridge, UK: Cambridge University Press)

Burlaga, L. F. 1995, Interplanetary Magnetohydrodynamics (New York: Oxford University Press)

Chhabra, A., & Jensen, R. V. 1989, Phys. Rev. Lett., 62, 1327

Chhabra, A. B., Meneveau, C., Jensen, R. V., & Sreenivasan, K. R. 1989, Phys. Rev. A, 40, 5284

Davis, T. M., & Lineweaver, C. H. 2004, Publications of the Astronomical Society of Australia, 21, 97–

Dressler, A. 1980, ApJS, 42, 565

Falconer, K. 1990, Fractal Geometry: Mathematical Foundations and Applications (J. Wiley: New York)

Frisch, U. 1995, Turbulence. The legacy of A.N. Kolmogorov (Cambridge UK: Cambridge University Press)

Gaite, J. 2021, Advances in Astronomy, 2021, 6680938

Huber, P. J. 1964, Annals Mathematical Statistics, 35, 73

Jones, B. J., Martínez, V. J., Saar, E., & Trimble, V. 2005, Rev. Modern Phys., 76, 1211

Jones, B. J. T., Martinez, V. J., Saar, E., & Einasto, J. 1988, ApJ, 332, L1

Jones, D. H., Read, M. A., Saunders, W., et al. 2009, MNRAS, 399, 683

Macek, W. M. 2007, Nonlinear Processes in Geophysics, 14, 695

—. 2020, The Origin of the World: Cosmos or Chaos? (Warsaw, Poland: Cardinal Stefan Wyszyński University (UKSW) Scientific Editions), in English, ISBN: 978-83-8090-686-0, e-ISBN: 978-83-8090-687-7.

Macek, W. M. 2022, in 14th Chaotic Modeling and Simulation International Conference, ed. C. H. Skiadas & Y. Dimotikalis (Cham: Springer International Publishing), 311–326

Macek, W. M., Krasińska, A., Silveira, M. V. D., et al. 2018, Astrophys. J. Lett., 864, L29

Macek, W. M., & Strumik, M. 2014, Phys. Rev. Lett., 112

Macek, W. M., & Wawrzaszek, A. 2009, J. Geophys. Res., 114

Macek, W. M., Wawrzaszek, A., & Burlaga, L. F. 2014, Astrophys. J. Lett., 793, L30

Macek, W. M., Wawrzaszek, A., & Carbone, V. 2011, Geophys. Res. Lett., 38, L19103

—. 2012, J. Geophys. Res., 117, 12101

Macek, W. M., Wójcik, D., & Burch, J. L. 2023, Astrophys. J., 943, 152

Maddox, J. 1987, Nature, 329, 195

Mandelbrot, B. B. 1982, The Fractal Geometry of Nature (Freeman, New York)

Martinez, V. J., Jones, B. J. T., Dominguez-Tenreiro, R., & van de Weygaert, R. 1990, Astrophys. J. Lett., 357, 50

Meneveau, C., & Sreenivasan, K. R. 1987, Phys. Rev. Lett., 59, 1424

Ott, E. 1993, Chaos in Dynamical Systems (Cambridge: Cambridge University Press)

Shectman, S. A., Landy, S. D., Oemler, A., et al. 1996, Astrophys. J. Lett., 470, 172

307 Skrutskie, M. F., Cutri, R. M., Stiening, R., et al. 2006, Astrophys. J., 131, 1163

308 Teles, S., Lopes, A., & Ribeiro, M. B. 2022, European Phys. J. C, 82, 896

309 Wójcik, D., & Macek, W. M. 2024, Phys. Rev. E., in press